

---

# Planar Ultrametric Rounding for Image Segmentation \*

---

**Julian Yarkony**  
 Experian Data Lab  
 San Diego, CA 92130  
 julian.yarkony@experian.com

**Charless C. Fowlkes**  
 Department of Computer Science  
 University of California Irvine  
 fowlkes@ics.uci.edu

## Abstract

We study the problem of hierarchical clustering on planar graphs. We formulate this in terms of an LP relaxation of ultrametric rounding. To solve this LP efficiently we introduce a dual cutting plane scheme that uses minimum cost perfect matching as a subroutine in order to efficiently explore the space of planar partitions. We apply our algorithm to the problem of hierarchical image segmentation.

## 1 Introduction

In this work, we formulate hierarchical image segmentation from the perspective of estimating an ultrametric over the set of image pixels that agrees closely with an input set of noisy pairwise distances. An ultrametric is a metric space in which the triangle inequality is replaced by the ultrametric inequality  $d(u, v) \leq \max\{d(u, w), d(v, w)\}$ . This inequality captures the transitive property of clustering (if  $u$  and  $w$  are in the same cluster and  $v$  and  $w$  are in the same cluster, then  $u$  and  $v$  must also be in the same cluster). Thresholding an ultrametric immediately yields a partition into sets whose diameter is less than the given threshold and varying the threshold naturally produces a hierarchical clustering in which clusters at high thresholds are composed of clusters at lower thresholds.

Inspired by the approach of [1], our method represents an ultrametric explicitly as a hierarchical collection of segmentations. Determining the appropriate segmentation at a single distance threshold is equivalent to finding a minimum-weight multicut in a graph with both positive and negative edge weights [3, 14, 2, 11, 20, 21, 4, 19, 7]. Finding an ultrametric imposes the additional constraint that these multcuts are hierarchically consistent across different thresholds. We focus on the case where the input distances are specified by a planar graph which arises naturally in the domain of image segmentation where elements are pixels or superpixels and distances are defined between neighbors. This allows us to exploit fast combinatorial algorithms for partitioning planar graphs that yield tighter LP relaxations than the local polytope relaxation [20].

This paper is organized as follows. We first introduce the ultrametric rounding problem and the relation between multcuts and ultrametrics. We then introduce a LP relaxation that uses a delayed column generation approach that exploits planarity to efficiently find cuts using the classic reduction to minimum-weight perfect matching [13, 8, 9, 10]. We apply our algorithm to the task of natural image segmentation on the Berkeley Segmentation Data Set benchmark [16]. We show compelling visual results and demonstrate that our algorithm converges rapidly and produces near optimal or optimal solutions in practice with guarantees.

---

\*JY acknowledges the support of Experian, CF acknowledges support of NSF grants IIS-1253538 and DBI-1262547

## 2 Ultrametric Rounding and Multicuts

Let  $G = (V, E)$  be a weighted graph with non-negative edge weights  $\theta$  indexed by edges  $e = (u, v) \in E$ . Our goal is to find an ultrametric distance  $d_{(u,v)}$  over vertices of the graph that is close to  $\theta$  in the sense that the distortion  $\sum_{(u,v) \in E} \|\theta_{(u,v)} - d_{(u,v)}\|_2^2$  is minimized. We begin by reformulating this rounding problem in terms of finding a set of nested multicuts in a family of weighted graphs.

We specify a partitioning or multicut of the vertices of the graph  $G$  into components using a binary vector  $\bar{X} \in \{0, 1\}^{|E|}$  where  $\bar{X}_e = 1$  indicates that the edge  $e = (u, v)$  is “cut” and that the vertices  $u$  and  $v$  associated with the edge are in separate components of the partition. We use  $\text{MCUT}(G)$  to denote the set of binary indicator vectors  $\bar{X}$  that represent valid multicuts of the graph  $G$ . For notational simplicity, in the remainder of the paper we frequently omit the dependence on  $G$  which is given as a fixed input.

A necessary and sufficient condition for an indicator vector  $\bar{X}$  to define a valid multicut in  $G$  is that for every cycle of edges, if one edge on the cycle is cut then at least one other edge in the cycle must also be cut. Let  $C$  denote the set of all cycles in  $G$  where each cycle  $c \in C$  is a set of edges and  $c - \hat{e}$  is the set of edges in cycle  $c$  excluding edge  $\hat{e}$ . We can express  $\text{MCUT}$  in terms of these *cycle inequalities* as:

$$\text{MCUT} = \left\{ \bar{X} \in \{0, 1\}^{|E|} : \sum_{e \in c - \hat{e}} \bar{X}_e \geq \bar{X}_{\hat{e}}, \forall c \in C, \hat{e} \in c \right\} \quad (1)$$

A hierarchical clustering of a graph can be described by a nested collection of multicuts. We denote the space of valid hierarchical partitions with  $L$  layers by  $\bar{\Omega}_L$  which we represent by a set of  $L$  edge-indicator vectors  $\mathcal{X} = (\bar{X}^1, \bar{X}^2, \bar{X}^3, \dots, \bar{X}^L)$  in which any cut edge remains cut at all finer layers of the hierarchy.

$$\bar{\Omega}_L = \{(\bar{X}^1, \bar{X}^2, \dots, \bar{X}^L) : \bar{X}^l \in \text{MCUT}, \bar{X}^l \geq \bar{X}^{l+1} \forall l\} \quad (2)$$

Given a valid hierarchical clustering  $\mathcal{X}$ , an ultrametric  $d$  can be specified over the vertices of the graph by choosing a sequence of real values  $0 = \delta^0 < \delta^1 < \delta^2 < \dots < \delta^L$  that indicate a distance threshold associated with each level  $l$  of the hierarchical clustering. The ultrametric distance  $d$  specified by the pair  $(\mathcal{X}, \delta)$  assigns a distance to each pair of vertices  $d_{(u,v)}$  based on the coarsest level of the clustering at which they remain in separate clusters. For pairs corresponding to an edge in the graph  $(u, v) = e \in E$  we can write this explicitly in terms of the multicut indicator vectors as:

$$d_e = \max_{l \in \{0, 1, \dots, L\}} \delta^l \bar{X}_e^l = \sum_{l=0}^L \delta^l [\bar{X}_e^l > \bar{X}_e^{l+1}] \quad (3)$$

We assume by convention that  $\bar{X}_e^0 = 1$  and  $\bar{X}_e^{L+1} = 0$ . Pairs  $(u, v)$  that do not correspond to an edge in the original graph can still be assigned a unique distance based on the coarsest level  $l$  at which they lie in different connected components of the cut specified by  $\bar{X}^l$ .

To compute the quality of an ultrametric  $d$  with respect to an input set of edge weights  $\theta$ , we measure the squared  $L_2$  difference between the edge weights and the ultrametric distance  $\|\theta - d\|_2^2$ . To write this compactly in terms of multicut indicator vectors, we construct a set of weights for each edge and layer, denoted  $\theta_e^l$  so that  $\sum_{l=0}^m \theta_e^l = \|\theta_e - \delta^m\|^2$ . These weights are given explicitly by the telescoping series:

$$\theta_e^0 = \|\theta_e\|^2 \quad \theta_e^l = \|\theta_e - \delta^l\|^2 - \|\theta_e - \delta^{l-1}\|^2 \quad \forall l > 1 \quad (4)$$

We use  $\theta^l \in R^{|E|}$  to denote the vector containing  $\theta_e^l$  for all  $e \in E$ .

For a fixed number of levels  $L$  and fixed set of thresholds  $\delta$ , the problem of finding the nearest ultrametric  $d$  can then be written as an integer linear program (ILP) over the edge cut indicators.

$$\begin{aligned}
\min_d \sum_{e \in E} \|\theta_e - d_e\|^2 &= \min_{\mathcal{X} \in \bar{\Omega}_L} \sum_{e \in E} \left\| \theta_e - \sum_{l=0}^L \delta^l [\bar{X}_e^l > \bar{X}_e^{l+1}] \right\|^2 \\
&= \min_{\mathcal{X} \in \bar{\Omega}_L} \sum_{e \in E} \sum_{l=0}^L \|\theta_e - \delta^l\|^2 (\bar{X}_e^l - \bar{X}_e^{l+1}) \\
&= \min_{\mathcal{X} \in \bar{\Omega}_L} \sum_{e \in E} \left( \|\theta_e\|^2 \bar{X}_e^0 + \sum_{l=1}^L (\|\theta_e - \delta^l\|^2 - \|\theta_e - \delta^{l-1}\|^2) \bar{X}_e^l + \|\theta_e - \delta^L\|^2 \bar{X}_e^{L+1} \right) \\
&= \min_{\mathcal{X} \in \bar{\Omega}_L} \sum_{l=0}^L \sum_{e \in E} \theta_e^l \bar{X}_e^l \\
&= \min_{\mathcal{X} \in \bar{\Omega}_L} \sum_{l=0}^L \theta^l \cdot \bar{X}^l
\end{aligned} \tag{5}$$

This optimization corresponds to solving a collection of minimum-weight multicut problems where the multicuts are constrained to be hierarchically consistent.

Computing minimum-weight multicuts (also known as correlation clustering) is NP hard even in the case of planar graphs [6]. A direct approach to finding an approximate solution to Eq 5 is to relax the integrality constraints on  $\bar{X}^l$  and instead optimize over the whole polytope defined by the set of cycle inequalities. We write CYC to indicate the polytope of real valued indicator vectors  $X$  that satisfy the cycle inequalities

$$\text{CYC} = \left\{ X \in [0, 1]^{|E|} : \sum_{e \in c - \hat{e}} X_e \geq X_{\hat{e}}, \forall c \in C, \hat{e} \in c \right\} \tag{6}$$

and use  $\Omega_L$  to denote the corresponding relaxation of  $\bar{\Omega}_L$  given by

$$\Omega_L = \{(X^1, X^2, \dots, X^L) : X^l \in \text{CYC}, X^l \geq X^{l+1} \forall l\}$$

While the polytope CYC contains non-integral vertices (it is not the convex hull of MCUT), the integral vertices of CYC do correspond exactly to the set of valid multicuts [12].

In practice, we found that applying a straightforward cutting-plane approach that successively adds violated cycle inequalities to this relaxation of Eq 5 requires far too many constraints and is too slow to be useful. Instead, we develop a column generation approach tailored for planar graphs that allows for efficient and accurate approximate inference.

### 3 The Cut Cone and Planar Multicuts

Consider a partition of a planar graph into two disjoint sets of nodes. We denote the space of indicator vectors corresponding to such two-way cuts by CUT. A cut may yield more than two connected components but it can not produce every possible multicut (e.g., it can not split a triangle of three nodes into three separate components). Let  $Z \in \{0, 1\}^{|E| \times |\text{CUT}|}$  be an indicator matrix where each column specifies a valid two-way cut with  $Z_{ek} = 1$  if and only if edge  $e$  is cut in two-way cut  $k$ . The indicator vector of any multicut in a planar graph can be generated by a suitable linear combination of cuts (columns of  $Z$ ) that isolate the individual components from the rest of the graph where the weight of each such cut is  $\frac{1}{2}$ .

Let  $\gamma \in \mathbb{R}^{|\text{CUT}|}$  be a vector specifying a positive weighted combination of cuts. The set  $\text{CUT}^\Delta = \{Z\gamma : \gamma \geq 0\}$  is the conic hull of CUT or “cut cone”. Since any multicut can be expressed as a superposition of cuts, the cut cone is identical to the conic hull of MCUT. This equivalence suggests an LP relaxation of the minimum-cost multicut given by

$$\min_{\gamma \geq 0} \theta \cdot Z\gamma \quad s.t. \quad Z\gamma \leq 1 \tag{7}$$

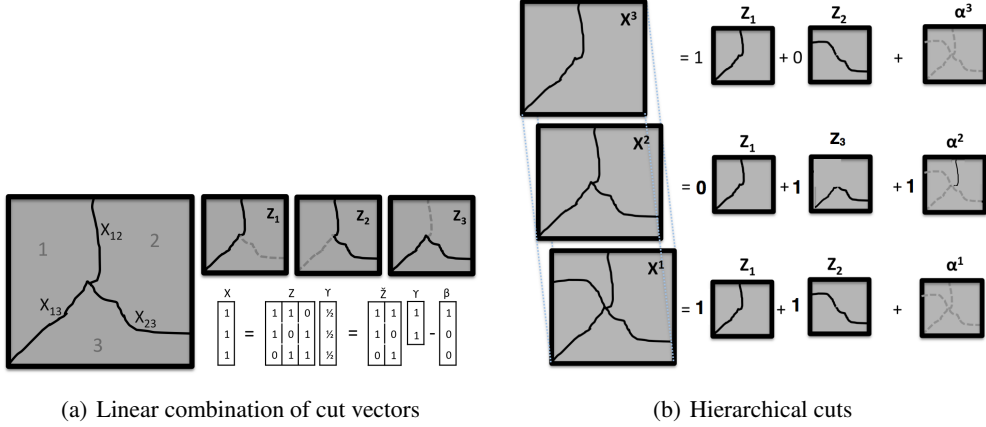


Figure 1: (a) Any partitioning  $X$  can be represented as a linear superposition of cuts  $Z$  where each cut isolates a connected component of the partition and is assigned a weight  $\gamma = \frac{1}{2}$  [20]. By introducing an auxiliary slack variables  $\beta$ , we are able to represent a larger set of valid indicator vectors  $X$  using fewer columns of  $Z$ . (b) By introducing additional slack variables at each layer of the hierarchical segmentation, we can efficiently represent many hierarchical segmentations (here  $\{X^1, X^2, X^3\}$ ) that are consistent from layer to layer while using only a small number of cut indicators as columns of  $Z$ .

where the vector  $\theta \in \mathbb{R}^{|E|}$  specifies the edge weights. For the case of planar graphs, any solution to this LP relaxation satisfies the cycle inequalities (see Appendix A and [12, 18, 10]).

**Expanded Multicut Objective:** Since the matrix  $Z$  contains an exponential number of cuts, Eq. 7 is still intractable. Instead we consider an approximation using a constraint set  $\hat{Z}$  which is a subset of columns of  $Z$ . In previous work [20], we showed that since the optimal multicut may no longer lie in the span of the reduced cut matrix  $\hat{Z}$ , it is useful to allow some values of  $\hat{Z}\gamma$  exceed 1 (see Figure 1(a) for an example).

We introduce a slack vector  $\beta \geq 0$  that tracks the presence of any “overcut” edges and prevents them from contributing to the objective when the corresponding edge weight is negative. Let  $\theta_e^- = \min(\theta_e, 0)$  denote the non-positive component of  $\theta_e$ . The expanded multi-cut objective is given by:

$$\min_{\substack{\gamma \geq 0 \\ \beta \geq 0}} \theta \cdot \hat{Z}\gamma - \theta^- \cdot \beta \quad \text{s.t.} \quad \hat{Z}\gamma - \beta \leq 1 \quad (8)$$

For any edge  $e$  such that  $\theta_e < 0$ , any decrease in the objective from overcutting by an amount  $\beta_e$  it is exactly compensated for in the objective by the term  $-\theta_e^- \beta_e$ .

When  $\hat{Z}$  contains all cuts (i.e.,  $\hat{Z} = Z$ ) then Eq 7 and Eq 8 are equivalent [20]. Further, if  $\gamma^*$  is the minimizer of Eq 8 when  $\hat{Z}$  only contains a subset of columns, then the edge indicator vector given by  $X = \min(1, \hat{Z}\gamma^*)$  still satisfies the cycle inequalities (see Appendix A for details).

## 4 Relaxing Ultrametric Rounding

To relax the ultrametric rounding problem, we replace the multicut problem at each layer  $l$  using the expanded multicut objective described by Eq 8. We let  $\gamma = \{\gamma^1, \gamma^2, \gamma^3 \dots \gamma^L\}$  and  $\beta = \{\beta^1, \beta^2, \beta^3 \dots \beta^L\}$  denote the collection of weights and slacks for the levels of the hierarchy and let  $\theta_e^{+l} = \max(0, \theta_e^l)$  and  $\theta_e^{-l} = \min(0, \theta_e^l)$  denote the positive and negative components

of  $\theta^l$ . We write the relaxed ultrametric rounding problem as:

$$\min_{\substack{\gamma \geq 0 \\ \beta \geq 0}} \sum_{l=1}^L (\theta^l \cdot Z\gamma^l - \theta^{-l} \cdot \beta^l) \quad (9)$$

$$\begin{aligned} \text{s.t. } & Z\gamma^{l+1} \leq Z\gamma^l \quad \forall l < L \\ & Z\gamma^l - \beta^l \leq 1 \quad \forall l \end{aligned} \quad (10)$$

where we have dropped the  $l = 0$  term from Eq 5 which is a constant.

**Expanded Ultrametric Cut Cone Objective:** As with Eq 8, it is computationally useful to introduce an additional slack vector associated with each level  $l$  and edge  $e$  which we denote as  $\alpha = \{\alpha^1, \alpha^2, \alpha^3 \dots \alpha^{L-1}\}$ . The introduction of  $\alpha_e^l$  allows for cuts represented by  $Z\gamma^l$  to violate the hierarchical constraint  $Z\gamma_e^l \geq Z\gamma_e^{l+1}$ . However we modify the objective so that violations to the original hierarchy constraint are paid for in proportion to  $\theta_e^{+l}$ . The introduction of  $\alpha$  allows us to find valid ultrametrics while using a smaller number of columns of  $Z$  to be used than would otherwise be required (illustrated in Figure 1(b)). We call this relaxed ultrametric rounding problem including the slack variable  $\alpha$  the *expanded ultrametric rounding objective*, written as:

$$\min_{\substack{\gamma \geq 0 \\ \beta \geq 0 \\ \alpha \geq 0}} \sum_{l=1}^L \theta^l \cdot Z\gamma^l + \sum_{l=1}^L -\theta^{-l} \cdot \beta^l + \sum_{l=1}^{L-1} \theta^{+l} \cdot \alpha^l \quad (11)$$

$$\begin{aligned} \text{s.t. } & Z\gamma^{l+1} + \alpha^{l+1} \leq Z\gamma^l + \alpha^l \quad \forall l < L \\ & Z\gamma^l - \beta^l \leq 1 \quad \forall l \end{aligned} \quad (12)$$

where by convention we define  $\alpha^L = 0$ .

Given a solution  $(\alpha, \beta, \gamma)$  we can recover a relaxed solution to the ultrametric rounding problem (Eq. 9) over  $\Omega^L$  by setting  $X_e^l = \min(1, \max_{m \geq l} (Z\gamma^m)_e)$ . In Appendix B, we demonstrate that for any  $(\alpha, \beta, \gamma)$  that obeys the constraints in Eq 11, this thresholding operation yields a solution  $\mathcal{X}$  that lies in  $\Omega^L$  and achieves the same or lower objective value.

## 5 The Dual Objective

We optimize the dual of the objective in Eq 11 using an efficient column generation approach based on perfect matching. A detailed derivation is given in Appendix C. Briefly, We introduce two sets of Lagrange multipliers  $\omega = \{\omega^1, \omega^2, \omega^3 \dots \omega^{L-1}\}$  and  $\lambda = \{\lambda^1, \lambda^2, \lambda^3 \dots \lambda^L\}$  corresponding to the between and within layer constraints respectively. For notational convenience, let  $\omega^0 = 0$ . The dual objective can then be written as

$$\begin{aligned} \max_{\omega \geq 0, \lambda \geq 0} & \sum_{l=1}^L -\lambda^l \cdot 1 \\ \theta^{-l} & \leq -\lambda^l \quad \forall l \\ -(\omega^{l-1} - \omega^l) & \leq \theta^{+l} \quad \forall l \\ (\theta^l + \lambda^l + \omega^{l-1} - \omega^l) \cdot Z & \geq 0 \quad \forall l \end{aligned} \quad (13)$$

The dual LP can be interpreted as finding a small modification of the original edge weights  $\theta^l$  so that every possible two-way cut of each resulting graph at level  $l$  has non-negative weight. Observe that the introduction of the two slack terms  $\alpha$  and  $\beta$  in the primal problem (Eq 11) results in bounds on the Lagrange multipliers  $\lambda$  and  $\omega$  in the dual problem in Eq 13. In practice these dual constraints turn out to be essential for efficient optimization and constitute the core contribution of this paper.

## 6 Solving the Dual via Cutting Planes

The chief complexity of the dual LP is contained in the constraints including  $Z$  which encodes non-negativity of an exponential number of cuts of the graph represented by the columns of  $Z$ . To

circumvent the difficulty of explicitly enumerating the columns of  $Z$ , we employ a cutting plane method that efficiently searches for additional violated constraints (columns of  $Z$ ) which are then successively added.

Let  $\hat{Z}$  denote the current working set of columns. Our dual optimization algorithm iterates over the following three steps: (1) Solve the dual LP with  $\hat{Z}$ , (2) find the most violated constraint of the form  $(\theta^l + \lambda^l + \omega^{l-1} - \omega^l) \cdot Z \geq 0$  for layer  $l$ , (3) Append a column to the matrix  $\hat{Z}$  for each such cut found. We terminate when no violated constraints exist or a computational budget has been exceeded.

### 6.1 Finding Violated Constraints

Identifying columns to add to  $\hat{Z}$  is carried out for each layer  $l$  separately. Finding the most violated constraint of the full problem corresponds to computing the minimum-weight cut of a graph with edge weights  $\theta^l + \lambda^l + \omega^{l-1} - \omega^l$ . If this cut has non-negative weight then all the constraints are satisfied, otherwise we add the corresponding cut indicator vector as an additional column of  $Z$ .

To generate a new constraint for layer  $l$  based on the current Lagrange multipliers, we solve

$$z^l = \arg \min_{z \in \text{CUT}} \sum_{e \in E} (\theta_e^l + \lambda_e^l + \omega_e^{l-1} - \omega_e^l) z_e \quad (14)$$

and subsequently add the new constraints from all layers to our LP,  $\hat{Z} \leftarrow [\hat{Z}, z^1, z^2, \dots, z^L]$ . Unlike the multicut problem, finding a (two-way) cut in a planar graph can be solved exactly by a reduction to minimum-weight perfect matching. This is a classic result that, e.g. provides an exact solution for the ground state of a 2D lattice Ising model without a ferromagnetic field [13, 8, 9, 10] in  $O(N^{\frac{3}{2}} \log N)$  time [15].

**Computing a lower bound:** At a given iteration, prior to adding a newly generated set of constraints we can compute the total residual constraint violation over all layers of hierarchy by  $\Delta = \sum_l (\theta^l + \lambda^l + \omega^{l-1} - \omega^l) \cdot z^l$ . In Appendix D we demonstrate that the value of the dual objective plus  $\frac{3}{2}\Delta$  is a lower-bound on the relaxed ultrametric rounding problem in Eq 11. Thus, as the costs of the minimum-weight matchings approaches zero from below, the objective of the reduced problem over  $\hat{Z}$  approaches an accurate lower-bound on optimization over  $\bar{\Omega}_L$ .

### 6.2 Implementation Details

**Expanding generated cut constraints:** When a given cut  $z^l$  produces more than two connected components, we found it useful to add a constraint corresponding to each component, following the approach of [20]. Let the number of connected components of  $z^l$  be denoted  $M$ . For each of the  $M$  components then we add one column to  $Z$ ; one corresponding to the cut that isolates each connected component from the rest. This allows more flexibility in representing the final optimum multicut as superpositions of these components. In addition, we also found it useful in practice to maintain a separate set of constraints  $\hat{Z}^l$  for each layer  $l$ . Maintaining independent constraints  $\hat{Z}^1, \hat{Z}^2, \dots, \hat{Z}^L$  can result in a smaller overall LP.

**Speeding convergence of  $\omega$ :** We found that adding an explicit penalty term to the objective that encourages small values of  $\omega$  speeds up convergence dramatically with no loss in solution quality. This penalty is scaled by a parameter  $\epsilon = 10^{-4}$  which is chosen to be extremely small in magnitude relative to the values of  $\theta$  so that it only has an influence when other no other “forces” are acting on a given term in  $\omega$ . With this refinement, the LP solved at each iteration of the cutting plane algorithm is given as follows.

$$\begin{aligned} \max_{\omega \geq 0, \lambda \geq 0} & \sum_{l=1}^L -\lambda^l 1 - \epsilon \|\omega\|_1 \\ \text{s.t. } & \theta^{-l} \leq -\lambda^l \quad \forall l \\ & -(\omega^{l-1} - \omega^l) \leq \theta^{+l} \quad \forall l \\ & (\theta^l + \lambda^l + \omega^{l-1} - \omega^l) Z \geq 0 \quad \forall l \end{aligned} \quad (15)$$

---

**Algorithm 1** Dual Ultrametric Rounding via Cutting Planes

---

```

 $\hat{Z}^l \leftarrow \{\}$   $\forall l$ , residual  $\leftarrow -\infty$ 
while residual  $< 0$  do
   $\{\omega\}, \{\lambda\} \leftarrow$  Solve Eq 15 given  $\hat{Z}$ 
  residual  $= 0$ 
  for  $l = 1 : L$  do
     $z^l \leftarrow \arg \min_{z \in \text{CUT}} (\theta^l + \lambda^l + \omega^{l-1} - \omega^l) \cdot z$ 
    residual  $\leftarrow$  residual +  $\frac{3}{2}(\theta^l + \lambda^l + \omega^{l-1} - \omega^l) \cdot z^l$ 
     $\{z(1), z(2), \dots, z(M)\} \leftarrow \text{isocuts}(z^l)$ 
     $\hat{Z}^l \leftarrow \hat{Z}^l \cup \{z(1), z(2), \dots, z(M)\}$ 
  end for
end while

```

---

### 6.3 Primal Decoding

Algorithm 1 gives a summary of the dual solver which at termination produces a lower-bound as well as a set of cuts described by the constraint matrices  $\hat{Z}^l$ . The subroutine *isocuts*( $z^l$ ) computes the set of cuts that isolate each connected component of  $z^l$

To generate a hierarchical clustering, we solve the primal, Eq 11, using this reduced set  $\hat{Z}$  in order to recover a fractional solution  $X_e^l = \min(1, \max_{m \geq l} (\hat{Z}^m \gamma^m)_e)$ . We use an LP solver (IBM CPLEX) which provides this primal solution “for free” when solving the dual in Algorithm 1.

We round this fractional solution to a discrete hierarchical clustering using a simple thresholding strategy. We threshold the fractional  $X$  as follows:  $\bar{X}_e^l \leftarrow [X_e^l > t]$ . We then repair any cut edges that lie inside a connected component by setting them to zero to assure that  $\bar{X}^l \in \text{MCUT}$ . In our implementation we test a few discrete thresholds  $t \in \{0, 0.2, 0.4, 0.6, 0.8\}$  and take that threshold that yields  $\bar{X}$  with the lowest cost. After each pass through the loop of Alg. 1 we compute these upper-bounds and retain the optimum solution observed thus far.

## 7 Experiments

We applied our algorithm on segmentation problems based on images from the Berkeley Segmentation Data set (BSDS) [16]. To construct our input graph we use superpixels generated by performing an oriented watershed transform on the output of the global probability of boundary (gPb) edge detector [17]. The vertices of the graph are superpixels and edges connect superpixels that are neighbors in the image, yielding a planar graph.

We construct base distance costs  $\theta$  by using the log-odds ratio of the local estimate of boundary contrast given by averaging *gPb* classifier output over the boundary between neighboring superpixels to yield a value  $gPb_e$ . We truncated extreme values to enforce that  $gPb_e \in [\epsilon, 1 - \epsilon]$  with  $\epsilon = 0.001$ . We set  $\theta_e = \log\left(\frac{1-gPb_e}{gPb_e}\right) + \log\left(\frac{1-\epsilon}{\epsilon}\right)$ . The additive offset assures that  $\theta_e \geq 0$ . In our experiments we use a fixed set of eleven distance threshold levels  $\{\delta_l\}$  that uniformly spanned the useful range of threshold values [9.6, 12.6]. We weighted edges proportionally to the length of the corresponding boundary in the image. We performed dual cutting plane iterations until convergence or 2000 seconds had passed. Lower-bounds for the BSDS segmentations were on the order of  $-10^3$  or  $-10^4$ . We terminate when the total residual is greater than  $-2 \times 10^{-4}$ . All codes were written in MATLAB using the Blossom V implementation of minimum-weight perfect matching [15] and the IBM ILOG CPLEX LP solver with default options.

### 7.1 Qualitative and Quantitative Results on Images

Figs 2, 3 show qualitative results for two images from the BSDS test data set. We display segmentations at eleven thresholds and color connected components of the segmentation at each layer with the average pixel color over that component. In Fig 4 we show the comparison of our ultrametric rounding algorithm (Alg 1, denoted UM) with the baseline ultrametric contour maps algorithm (UCM)

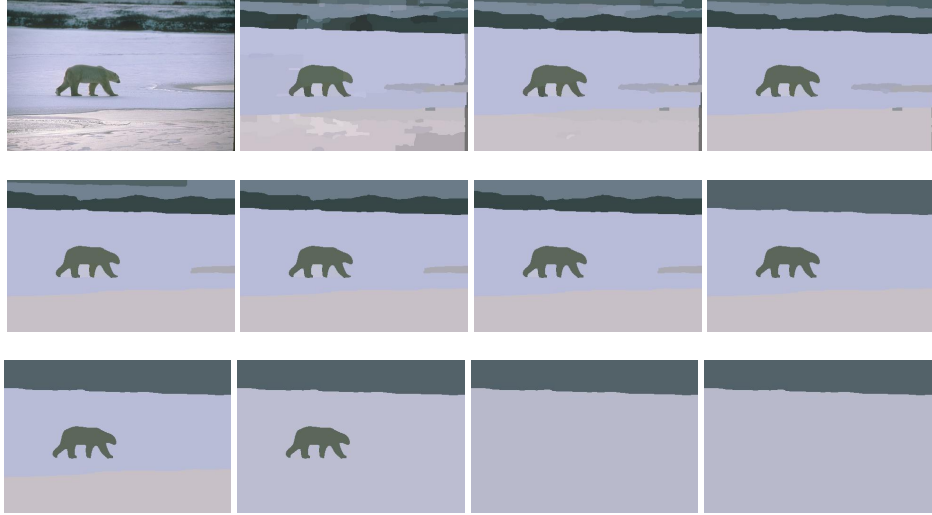


Figure 2: Top left to bottom right: A hierarchical image segmentation for a BSDS test set image showing eleven layers listed from fine to coarse. The original image is in the top left.

with and without length weighting [5]. UCM performs agglomerative clustering algorithm, successively merging segments with small boundary strengths to produce a hierarchical segmentation. We display a precision recall plot on the Berkeley Segmentation Data Set test set.

In terms of segmentation accuracy, UM rounding performs nearly identically to the state of the art UCM algorithm with regards to precision recall which is the standard measure employed in the literature. However we show some improvements in high precision range of the curve which corresponds to the coarse segmentations. It is worth noting that the BSDS benchmark does not provide strong penalties for small leaks between two segments when the total number of boundary pixels involved is small. Our algorithm may find strong application in domains where the local boundary signal is noisier (e.g., biological imaging) or when under-segmentation is more heavily penalized.

## 7.2 Objective Cost and Timing Experiments

In Fig 5,6,we display plots demonstrating the performance of the optimization routine according to eight different measures. The most interesting is the quality of the integer solution. We found the upper-bound given by the cost of the decoded integer solution and the lower-bound estimated by the dual LP are very close. The magnitude of the integrality gap is typically less than 0.1% of the magnitude of the lower-bound and never more than 1%. Convergence of the dual is achieved quite rapidly; most instances require less than 100 iterations to converge with roughly linear growth in the size of the LP at each iteration as cutting planes are added.

## 7.3 Cost Comparison with Ultrametric Contour Maps

We also compared the ultrametric rounding cost of solutions generated by our approach with costs associated with hierarchical clusterings produced by the Ultrametric Contour Map (UCM) length-weighted clusterings. This test is perhaps unfair as UCM was not necessarily designed to minimize the ultrametric rounding cost but provides a baseline for understanding the rounding objective.

UCM provides an ultrametric solution denoted  $U \in R^{|E|}$  where  $U$  is indexed by  $e$  and scaled to lie in the range  $[0, 1]$  with smaller values indicating lower likelihood of a boundary. For each level  $l$ , we select a threshold  $q \in [0, 1]$  which is used to threshold the UCM ultrametric  $U$ . We choose a value for  $q$  which minimizes the ultrametric rounding error, formally written as:

$$\min_{q^l} \sum_{e \in E} \theta_e^l [U_e > q^l] \quad (16)$$

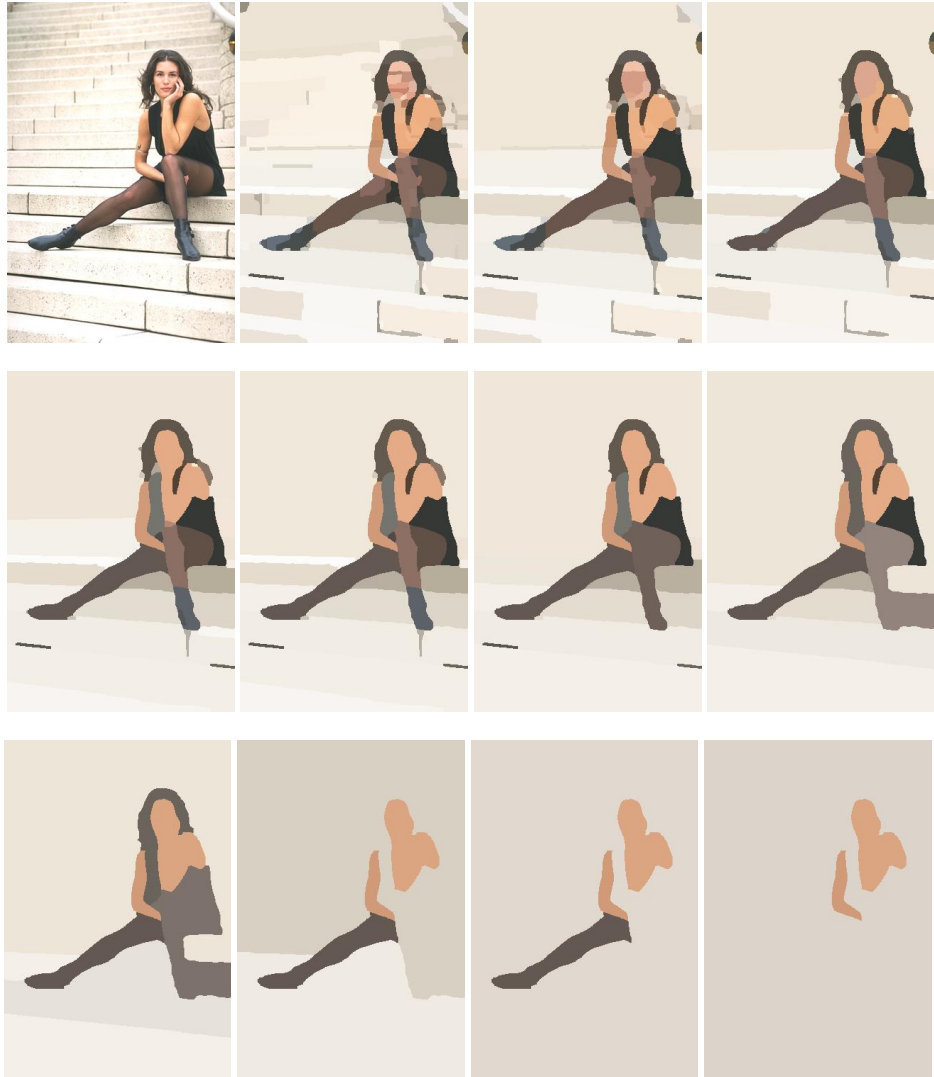


Figure 3: Top left to bottom right: A hierarchical image segmentation for a BSDS test set image showing eleven layers listed from fine to coarse. The original image is in the top left.

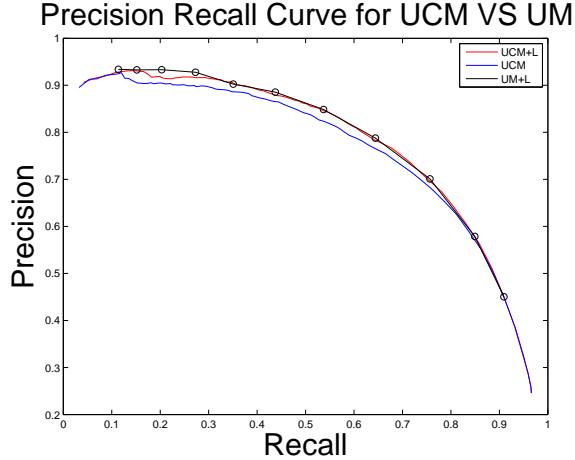


Figure 4: We show the comparison of our ultrametric rounding algorithm (UM) with the baseline ultrametric contour maps algorithm (UCM) with and without length weighting [5]. We display precision recall plots on the Berkeley Segmentation Data Set (BSDS). Observe that UM performs nearly identically to the state of the art UCM algorithm with regards to precision recall. However we do observe small but significant improvements in high precision range of the curve. We note the points plotted on the precision recall curve for UM with black dots. Use of length weighted costs are indicated by  $+L$ .

Thus the total cost for a given image is:

$$\sum_{l=1}^L \min_{q^l} \sum_{e \in E} \theta_e^l [U_e > q^l] \quad (17)$$

Observe that  $\theta_e^l < \theta_e^{l+1}$  and thus we are guaranteed  $q_e^l \leq q_e^{l+1}$ .

In Fig 7 we display a histogram, computed over test image problem instances, of the cost of UCM solutions relative to those produced by UM rounding. A value of 1 indicates equality. A value of greater than 1 indicates UCM providing lower cost while a value less than 1 indicated UM providing lower cost. In no instance did UCM outperform our UM algorithm though our UM algorithm often outperformed UCM.

#### 7.4 Segmentation performance and running time

While our cutting-plane approach is slower than agglomerative clustering, it is not necessary to wait for convergence in order to produce high quality results. We found that while the upper and lower bounds decrease as a function of time the clustering performance as measured by precision-recall stabilized is often nearly optimal after only ten seconds and is very stable after that. We show PR curves at several time points in Fig 8. In Fig 9 we shows a plot of the maximum f-measure of UM rounding as a function of time relative to the final values of UCM with and without length weighting.

#### 7.5 Importance of enforcing hierarchical constraints

Although independently finding multicut at different thresholds often produces hierarchical clusterings, this is by no means guaranteed. We ran Algorithm 1 while enforcing that  $\omega_e^l = 0 \forall [e \in E, l]$ . This allows the multicut problem for each layer to be solved independently as if the others did not exist. To solve these multicut problem instances we used the solver of [20]. In our data set of 200 images and 11 layers per problem results in 2200 total multicut instances. The less constrained single-layer solver produced a lower or equal cost multicut compared to the hierarchical solver in 99.77 percent of problem instances. In Fig 10 we show examples of hierarchy constraints being violated severely on multiple images when solving with  $\omega$  forced to zero. Introduction of the hierarchy constraint fixes such errors.

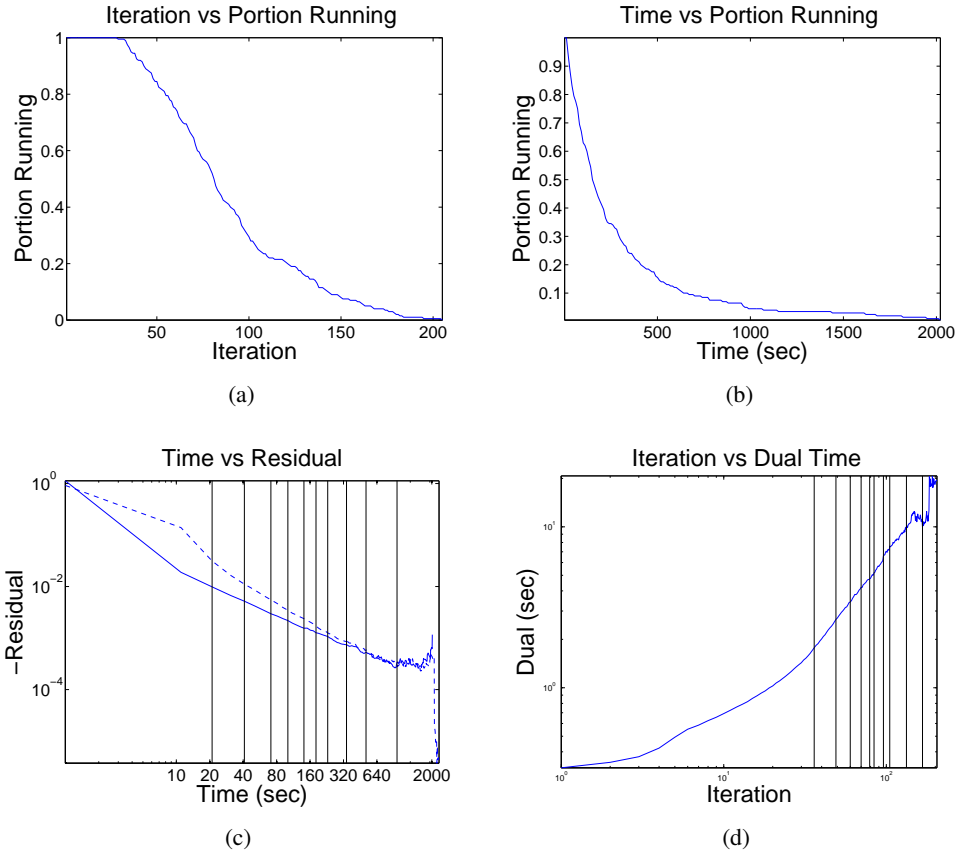


Figure 5: (a) We display the portion of the problems that have not terminated as a function of cutting-plane iteration. We observe that dual optimization always requires the solution of at least a few LP's for most problems to converge. (b) We display the portion of the problems that have not terminated as a function of time. We observe that dual optimization terminates rapidly for most problem instances. (c) We plot the value of the average residual constraint violation as a function of time averaged over images that have yet to terminate. Instances that terminated before 2000 seconds passed have residuals on the order of  $10^{-6}$  or less. We plot the best observed value in solid blue and the current value with dotted blue. We normalize the residual for a given instance by dividing by the magnitude of the tightest lower bound for that instance. We indicate the portion of instances that have yet to terminate using black bars. The bars are associated with the percent of instances incomplete with the bars from left to right being [95,85,75,65,...,5]. Observe that the value of the residual decays rapidly. (d) We plot the average amount of time per cutting-plane iteration. This includes solving one LP and finding the most violated constraint and extracting cuts for each layer. We use black bars as in (c) to indicate the percent of problems instances that have not terminated after a given time point.

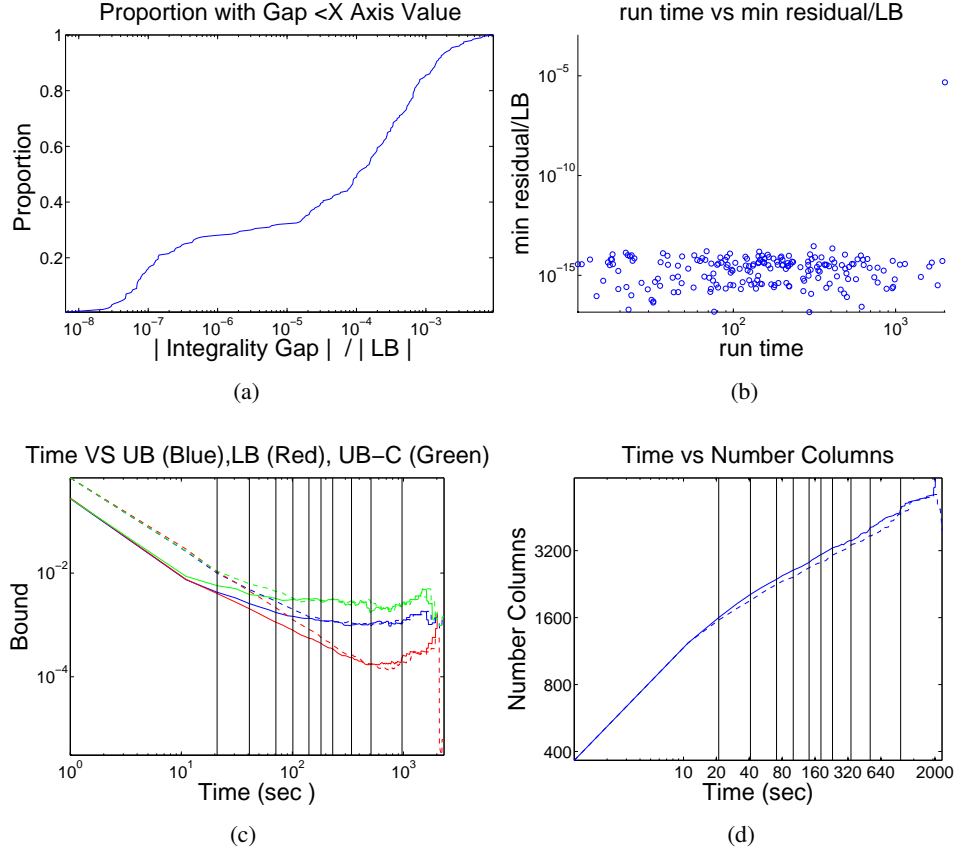


Figure 6: **(a)** We show a plot over image problem instances that describes the gap between the maximum lower bound computed for that image and the final rounded integral solution. To normalize the energy gap, we scale by the value of the maximum lower bound identified for that problem instance. We observe that the rounded integer solutions are near exact or exact on all images. **(b)** Scatter plot of the run time in (sec) versus the minimum magnitude residual (residual is always non-positive). We normalize this by dividing by the maximum lower bound over the coarse optimization (denoted LB) of the problem instance. Residual was negligible for all except 1 of 200 problem instances which did not terminate within 2000 seconds. **(c)**: We show the value of the integer solution and lower bound as a function of time averaged over problem instances. We normalize by computing the absolute value of the gap between each bound and the magnitude of the maximum lower bound discovered. We plot the value of the upper/lower bounds in blue/red. We plot in green the value of the integer solution but include time for rounding the solution after each iteration. We use dotted/solid lines to indicate the current/best value observed thus far. We indicate the percentage of instances that have yet to terminate using black bars marking [95, 85, 75, 65, ..., 5] percent. **(d)** We show the number of constraints (columns of  $\hat{Z}^l$  summed over layers and averaged over problem instances) as a function of running time. We use black bars as in **c** to indicate the proportion of the problems instances that have not converged at a given time point.

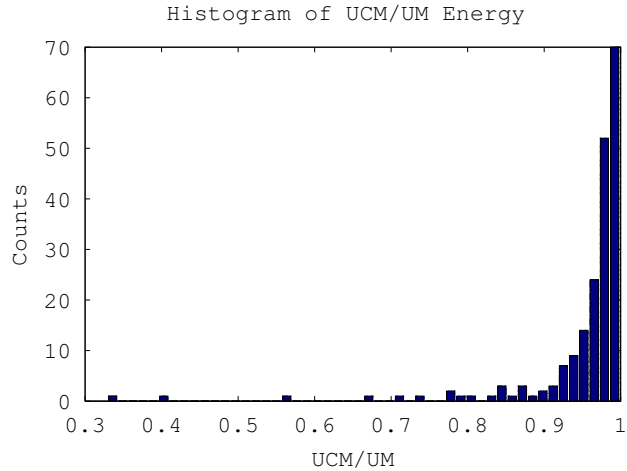


Figure 7: We compare the quality of the ultrametric rounding produced by our ultrametric rounding (UM) with the baseline ultrametric contour maps algorithm (UCM) in terms of the ultrametric rounding objective. We plot a histogram of the ratio of objective values of UCM and UM. All ratios were less than 1 showing that in no instances did UM produce a worse solution than UCM

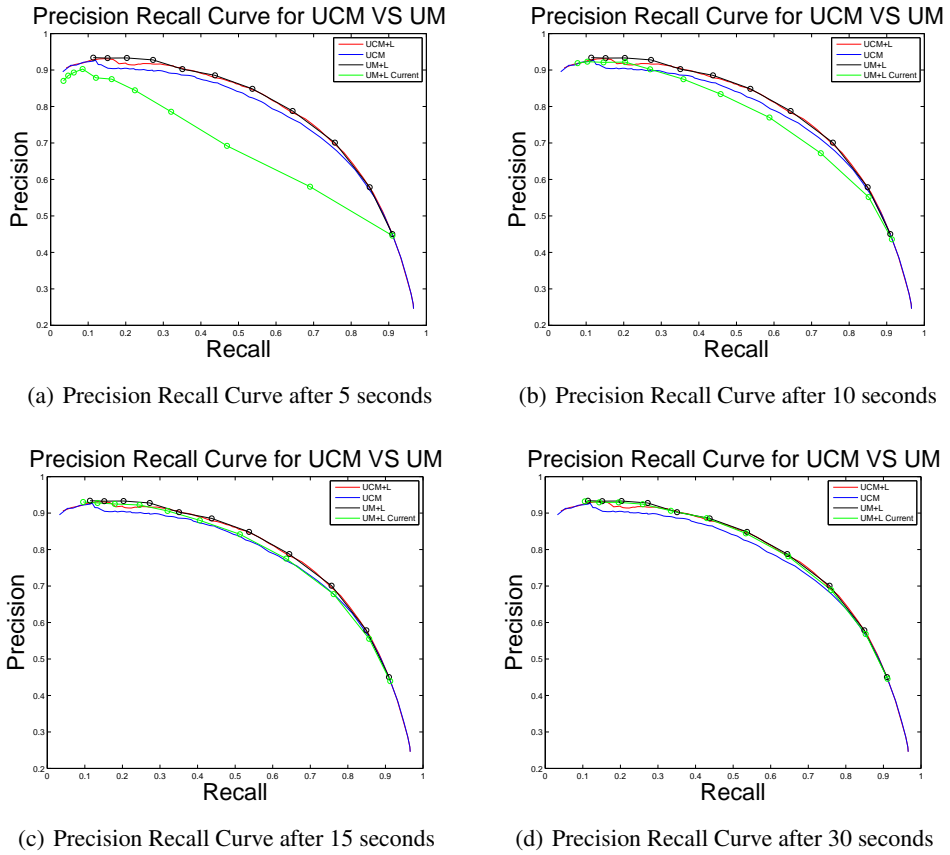


Figure 8: Anytime performance: We show the precision-recall curve of for segmentations derived from the lowest-cost solution decoded at a particular amount of execution time (green curves), stopping at  $T=5, 10, 15$  and  $30$  seconds respectively. We conclude that high-tolerance numerical convergence is not necessary to achieve good quality segmentations. For comparison, we plot the UCM with and without length weighting in red and blue respectively and the UM results after all problems terminate in black.

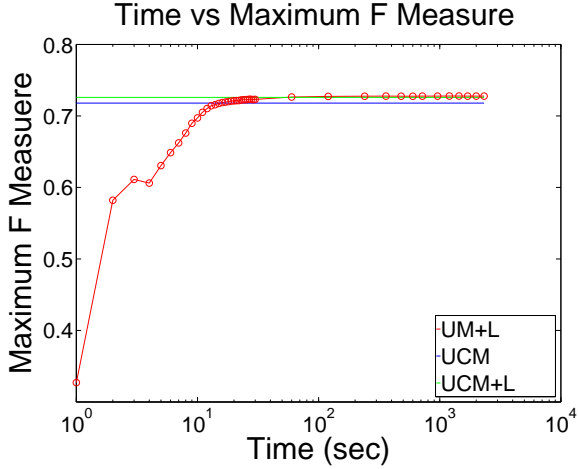


Figure 9: Anytime performance: We plot the maximum F-measure on the BSDS benchmark as a function of run-time. Clock time includes lower-bound optimization and upper-bound decoding after each iteration. We also include the maximum F-measure produced by UCM with and without length weighting. The final F-measures achieved by UCM, UCM+L and UM are 0.728, 0.726, 0.718 respectively.

## 8 Conclusion

We have introduced a new method for ultrametric rounding on planar graphs that is applicable to hierarchical image segmentation. Our contribution is a dual cutting plane approach that exploits the introduction of novel slack terms that allow for representing a much larger space of solutions with relatively few cutting planes. This yields an efficient algorithm that provides rigorous bounds on the quality the resulting solution. We empirically observe that our algorithm rapidly produces compelling image segmentations along with lower- and upper-bounds that are nearly tight on the benchmark BSDS test data set.

## References

- [1] Nir Ailon and Moses Charikar. Fitting tree metrics: Hierarchical clustering and phylogeny. In *Foundations of Computer Science, 2005. FOCS 2005. 46th Annual IEEE Symposium on*, pages 73–82. IEEE, 2005.
- [2] Bjoern Andres, Joerg H. Kappes, Thorsten Beier, Ullrich Kothe, and Fred A. Hamprecht. Probabilistic image segmentation with closedness constraints. In *Proceedings of the Fifth International Conference on Computer Vision (ICCV-11)*, pages 2611–2618, 2011.
- [3] Bjoern Andres, Thorben Kroger, Kevin L. Briggman, Winfried Denk, Natalya Korogod, Graham Knott, Ullrich Kothe, and Fred. A. Hamprecht. Globally optimal closed-surface segmentation for connectomics. In *Proceedings of the Twelfth International Conference on Computer Vision (ECCV-12)*, 2012.
- [4] Bjoern Andres, Julian Yarkony, B. S. Manjunath, Stephen Kirchhoff, Engin Turetken, Charless Fowlkes, and Hanspeter Pfister. Segmenting planar superpixel adjacency graphs w.r.t. non-planar superpixel affinity graphs. In *Proceedings of the Ninth Conference on Energy Minimization in Computer Vision and Pattern Recognition (EMMCVPR-13)*, 2013.
- [5] Pablo Arbelaez, Michael Maire, Charless Fowlkes, and Jitendra Malik. Contour detection and hierarchical image segmentation. *IEEE Trans. Pattern Anal. Mach. Intell.*, 33(5):898–916, May 2011.
- [6] Yoram Bachrach, Pushmeet Kohli, Vladimir Kolmogorov, and Morteza Zadimoghaddam. Optimal coalition structures in graph games. *CoRR*, abs/1108.5248, 2011.

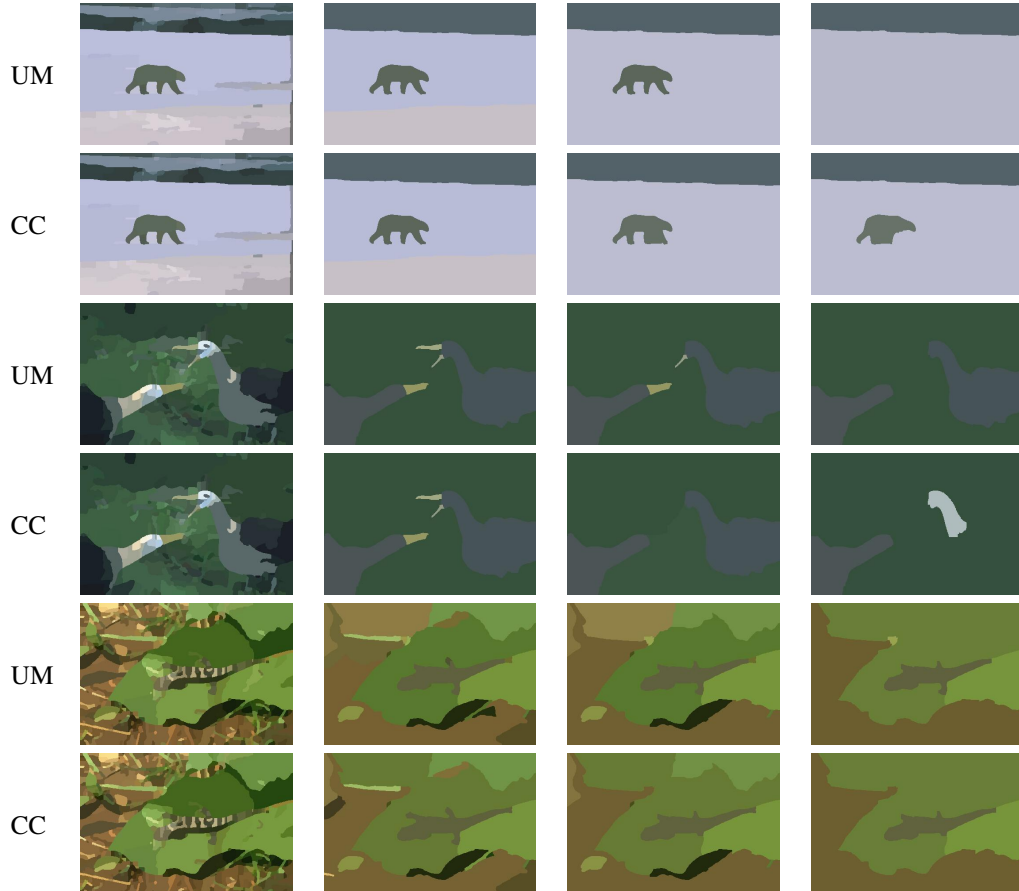


Figure 10: Examples where hierarchically nested segmentations give more semantically meaningful groupings of the image. The proposed ultrametric rounding (UM) enforces consistency across levels while performing independent correlation clustering (CC) at each threshold does not guarantee a hierarchical segmentation (c.f. first image). In the second image, hierarchical segmentation (UM) preserves semantic parts of the two birds while merging the background regions. In the third image, CC merges the background clutter into foreground leaf region at a very low threshold due to a single weak edge.

- [7] Shai Bagon and Meirav Galun. Large scale correlation clustering. In *CoRR, abs/1112.2903*, 2011.
- [8] F Barahona. On the computational complexity of ising spin glass models. *Journal of Physics A: Mathematical, Nuclear and General*, 15(10):3241–3253, april 1982.
- [9] F Barahona. On cuts and matchings in planar graphs. *Mathematical Programming*, 36(2):53–68, november 1991.
- [10] F Barahona and A Mahjoub. On the cut polytope. *Mathematical Programming*, 60(1-3):157–173, September 1986.
- [11] Thorsten Beier, Thorben Kroeger, Jorg H Kappes, Ullrich Kothe, and Fred A Hamprecht. Cut, glue, and cut: A fast, approximate solver for multicut partitioning. In *Computer Vision and Pattern Recognition (CVPR), 2014 IEEE Conference on*, pages 73–80, 2014.
- [12] Michel Deza and Monique Laurent. *Geometry of cuts and metrics*, volume 15. Springer Science & Business Media, 1997.
- [13] Michael E. Fisher. On the dimer solution of planar ising models. *Journal of Mathematical Physics*, 7(10):1776–1781, 1966.
- [14] Sungwoong Kim, Sebastian Nowozin, Pushmeet Kohli, and Chang Dong Yoo. Higher-order correlation clustering for image segmentation. In *Advances in Neural Information Processing Systems*, 25, pages 1530–1538, 2011.
- [15] Vladimir Kolmogorov. Blossom v: a new implementation of a minimum cost perfect matching algorithm. *Mathematical Programming Computation*, 1(1):43–67, 2009.
- [16] David Martin, Charless Fowlkes, Doron Tal, and Jitendra Malik. A database of human segmented natural images and its application to evaluating segmentation algorithms and measuring ecological statistics. In *Proceedings of the Eighth International Conference on Computer Vision (ICCV-01)*, pages 416–423, 2001.
- [17] David R. Martin, Charless C. Fowlkes, and Jitendra Malik. Learning to detect natural image boundaries using local brightness, color, and texture cues. *IEEE Trans. Pattern Anal. Mach. Intell.*, 26(5):530–549, May 2004.
- [18] Julian Yarkony. Analyzing planarcc. *NIPS 2014 workshop*, 2014.
- [19] Julian Yarkony, Thorsten Beier, Pierre Baldi, and Fred A Hamprecht. Parallel multicut segmentation via dual decomposition. In *New Frontiers in Mining Complex Patterns (NFMCP 2014)*, 2014.
- [20] Julian Yarkony, Alexander Ihler, and Charless Fowlkes. Fast planar correlation clustering for image segmentation. In *Proceedings of the 12th European Conference on Computer Vision (ECCV 2012)*, 2012.
- [21] Chong Zhang, Julian Yarkony, and Fred A. Hamprecht. Cell detection and segmentation using correlation clustering. In *Medical Image Computing and Computer-Assisted Intervention MICCAI 2014*, volume 8673, pages 9–16, 2014.

## A Expanded multicut objective and the cycle inequalities

In this appendix we show that for planar graphs, solving the expanded multicut optimization produces solutions that satisfy the cycle inequalities and have equivalent cost when truncated to lie in the unit hypercube. This establishes an equivalence between the expanded multicut optimization

$$\min_{\substack{\gamma \geq 0 \\ \beta \geq 0}} \theta \cdot \hat{Z}\gamma - \theta^- \cdot \beta \quad \text{s.t. } \hat{Z}\gamma - \beta \leq 1 \quad (18)$$

and the cycle polytope relaxation

$$\min_{X \in \text{CYC}} \theta \cdot X \quad (19)$$

for the case of planar graphs.

### A.1 Multicut cone and Cycle cone

Recall that  $\text{CUT}$  and  $\text{MCUT}$  denote the set of binary indicator vectors that represent valid two-way cuts and multcuts respectively for a specified graph  $G$ . We denote the conic hulls of these sets by

$$\text{CUT}^\Delta = \left\{ \sum_i X^i \gamma_i : \gamma_i \geq 0, X^i \in \text{CUT} \right\} \quad (20)$$

$$\text{MCUT}^\Delta = \left\{ \sum_i X^i \gamma_i : \gamma_i \geq 0, X^i \in \text{MCUT} \right\} \quad (21)$$

(22)

Finally, we denote the cone of positive vectors satisfying the cycle inequalities by:

$$\text{CYC}^\Delta = \left\{ X \geq 0, \sum_{e \in c - \hat{e}} X_e \geq X_{\hat{e}}, \forall c \in C, \hat{e} \in c \right\} \quad (23)$$

We now state a two basic results concerning these cones.

**Proposition 1:**  $\text{MCUT}^\Delta = \text{CUT}^\Delta$

Every cut indicator is a multicut indicator, hence  $\text{CUT}^\Delta \subset \text{MCUT}^\Delta$ . On the other hand, any multicut  $X \in \text{MCUT}$  can be written as a conic combination of cuts that isolate each connected component with weight  $\frac{1}{2}$  so that  $X = \frac{1}{2} \sum_i Z^i$  with  $Z^i \in \text{CUT}$  so  $\text{MCUT} \subset \text{CUT}^\Delta$  and hence  $\text{MCUT}^\Delta \subset \text{CUT}^\Delta$ .

**Proposition 2:** If  $G$  is planar,  $\text{CUT}^\Delta = \text{CYC}^\Delta$

A stronger version of this result due to [10] states that for a graph  $G$  containing no  $K_5$  minor, the set of cycle inequalities over chordless circuits is sufficient to specify the facets of the cut polytope for  $G$ . See [12] (p. 434) for a detailed discussion.

### A.2 The projected solution $\min(1, Z\gamma)$ satisfies the cycle inequalities

As a result of the basic properties of the cut cone, for any  $\gamma \geq 0$ , we have  $Z\gamma \in \text{CYC}^\Delta$  for planar graphs. Let  $X = \min(1, Z\gamma)$  be a solution to the expanded multicut objective and  $(Z\gamma)_e$  denote the value for a particular edge  $e$ . It must then be that  $X \in \text{CYC}^\Delta$  since:

$$\sum_{e \in c - \hat{e}} \min(1, (Z\gamma)_e) \geq \min(1, \sum_{e \in c - \hat{e}} (Z\gamma)_e) \quad (24)$$

$$\geq \min(1, (Z\gamma)_{\hat{e}}) \quad \forall c \in C, \hat{e} \in c \quad (25)$$

The first inequality arises from pulling the  $\min$  outside the sum. The second inequality holds since  $Z\gamma \in \text{CYC}^\Delta$

### A.3 The projected solution $\min(1, Z\gamma)$ achieves an objective cost no greater than that of $Z\gamma$

We now demonstrate that the fractional multicut  $X = \min(1, Z\gamma)$  given by projecting the solution  $Z\gamma$  yields a solution with an equal or smaller objective value.

Recall that  $\beta$  is a positive slack variable that allows corresponding edge indicators to take on a value greater than 1.

$$Z\gamma - \beta \leq 1 \quad (26)$$

Since the objective is non-decreasing in  $\beta$ , for a given setting of  $\gamma$  an optimal setting of the slack variables is given by:

$$\beta^* = \max(0, Z\gamma - 1) \quad (27)$$

We split the objective into positive and negative edges and write:

$$\theta \cdot Z\gamma - \theta^- \cdot \beta = \theta^+ \cdot Z\gamma + \theta^- \cdot Z\gamma - \theta^- \cdot \beta \quad (28)$$

$$= \theta^+ \cdot Z\gamma + \theta^- \cdot \min(1, Z\gamma) \quad (29)$$

$$\geq \theta^+ \cdot \min(1, Z\gamma) + \theta^- \cdot \min(1, Z\gamma) \quad (30)$$

$$= \theta \cdot \min(1, Z\gamma) \quad (31)$$

$$= \theta \cdot X \quad (32)$$

which establishes that projecting  $Z\gamma$  onto the unit cube yields a fractional multicut solution that does not increase the objective.

## B Expanded ultrametric objective and fractional ultrametrics

Recall the set of fractional ultrametrics is defined as follows

$$\Omega_L = \{ \{X^1, X^2, \dots, X^L\} : X^l \in \text{CYC}, X^l \geq X^{l+1} \forall l \} \quad (33)$$

In analogy with the previous appendix, we show the equivalence of the expanded ultrametric rounding problem:

$$\min_{\substack{\gamma \geq 0 \\ \beta \geq 0 \\ \alpha \geq 0}} \sum_{l=1}^L \theta^l \cdot Z\gamma^l + \sum_{l=1}^L -\theta^{-l} \cdot \beta^l + \sum_{l=1}^{L-1} \theta^{+l} \cdot \alpha^l \quad (34)$$

$$\text{s.t. } Z\gamma^{l+1} + \alpha^{l+1} \leq Z\gamma^l + \alpha^l \quad \forall l < L \\ Z\gamma^l - \beta^l \leq 1 \quad \forall l \quad (35)$$

with the relaxed problem:

$$\min_{x \in \Omega_L} \sum_{l=1}^L \theta^l \cdot X^l \quad (36)$$

Given an optimal solution to the expanded ultrametric rounding problem specified by  $(\gamma, \alpha, \beta)$ , we produce a fractional ultrametric  $H$  by the projection operation:

$$H^l = \min(1, \max_{m \geq l}(Z\gamma^m)) = \max(H^{l+1}, \min(1, (Z\gamma^l))) \quad (37)$$

We show that the resulting projection  $H$  yields a valid fractional ultrametric  $H \in \Omega_L$  whose cost is no greater than the cost of the corresponding solution to the expanded objective.

### B.1 Projecting expanded solutions into $\Omega_L$

By construction,  $H$  satisfies the hierarchical constraint  $H^l \geq H^{l+1}$ . We show that  $H^l \in \text{CYC}$  by induction. In the previous appendix, we established that  $H^L = \min(1, Z\gamma^L) \in \text{CYC}$ . Observe that each  $H^l$  for  $l < L$  is the coordinate-wise max of  $H^{l+1}$  and  $\min(1, Z\gamma^l)$ , both of which are in  $\text{CYC}$  so we only need show that  $\text{CYC}$  is closed under coordinate-wise maximum.

Let  $X^1$  and  $X^2$  be two elements of  $\text{CYC}$  and  $X^3 = \max(X^1, X^2)$ . We have  $\forall c \in C, \hat{e} \in c$

$$\sum_{e \in c - \hat{e}} X_e^3 = \sum_{e \in c - \hat{e}} \max(X_e^1, X_e^2) \quad (38)$$

$$\geq \max\left(\sum_{e \in c - \hat{e}} X_e^1, \sum_{e \in c - \hat{e}} X_e^2\right) \quad (39)$$

$$\geq \max(X_{\hat{e}}^1, X_{\hat{e}}^2) = X_{\hat{e}}^3 \quad (40)$$

$$(41)$$

where the first inequality arises from pulling the max outside the sum and the second because  $X^1$  and  $X^2$  each satisfy the cycle inequality. Hence  $X^3 \in \text{CYC}$ .

## B.2 The cost of $H$ is no greater than that of $\{\gamma, \alpha, \beta\}$

Fixing an optimal solution to the expanded ultrametric problem specified by  $\gamma$  we first note that the optimal values of  $\beta$  and  $\alpha$  are given by:

$$\beta^l = \max(0, Z\gamma^l - 1) \quad (42)$$

$$\alpha^l = \max_{m \geq l} (Z\gamma^m - Z\gamma^l) \quad (43)$$

The formula for  $\alpha$  can be developed by starting from layer  $L$  and working down, setting  $\alpha$  to the smallest possible value needed to satisfy the inter-layer constraints for a given  $\gamma$ .

$$\begin{aligned} \alpha^L &= 0 \\ \alpha^{L-1} &= \max(0, Z\gamma^L - Z\gamma^{L-1}) \\ \alpha^{L-2} &= \max(0, Z\gamma^L - Z\gamma^{L-2}, Z\gamma^{L-1} - Z\gamma^{L-2}) \\ &\dots \end{aligned} \quad (44)$$

Since the objective is non-decreasing in  $\alpha$  and  $\beta$ , these values are the smallest values for which the constraints are satisfied.

Plugging in the settings of the slack variables for each layer  $l$  we have:

$$\begin{aligned} \theta^l \cdot Z\gamma^l - \theta^{-l} \cdot \beta^l + \theta^{+l} \cdot \alpha^l &= (\theta^{+l} + \theta^{-l}) \cdot Z\gamma^l - \theta^{-l} \cdot \max(0, Z\gamma^l - 1) + \theta^{+l} \cdot \max_{m \geq l} (Z\gamma^m - Z\gamma^l) \\ &= \theta^{+l} \cdot (Z\gamma^l + \max_{m \geq l} (Z\gamma^m - Z\gamma^l)) + \theta^{-l} \cdot (Z\gamma^l - \max(0, Z\gamma^l - 1)) \\ &= \theta^{+l} \cdot \max_{m \geq l} Z\gamma^m + \theta^{-l} \cdot \min(1, Z\gamma^l) \\ &\geq \theta^{+l} \cdot \min(1, \max_{m \geq l} Z\gamma^m) + \theta^{-l} \cdot \min(1, Z\gamma^l) \\ &\geq \theta^{+l} \cdot \min(1, \max_{m \geq l} Z\gamma^m) + \theta^{-l} \cdot \min(1, \max_{m \geq l} Z\gamma^m) \\ &= \theta^l \cdot H^l \end{aligned}$$

where the second inequality holds because the max introduced is multiplied by a negative weight. Since projection can only remain the same or decrease the cost of each layer, the total objective must also be no greater than the expanded solution:

$$\sum_l \theta^l \cdot Z\gamma^l - \theta^{-l} \cdot \beta^l + \theta^{+l} \cdot \alpha^l \geq \sum_l \theta^l \cdot H^l$$

## C Derivation of Dual Problem

Here we give a derivation of the dual objective over the expanded ultrametric cut cone which we utilize to provide an efficient column generation approach based on perfect matching.

We introduce two sets of Lagrange multipliers  $\{\omega^1 \dots \omega^{L-1}\}$  and  $\{\lambda^1 \dots \lambda^L\}$  corresponding to the positivity constraints in Eq 11.

$$\begin{aligned} \min_{\substack{\gamma \geq 0 \\ \beta \geq 0 \\ \alpha \geq 0}} \max_{\substack{\omega \geq 0, \lambda \geq 0}} & \sum_{l=1}^L \theta^l Z \cdot \gamma^l - \sum_{l=1}^L \theta^{-l} \beta^l + \sum_{l=1}^{L-1} \theta^{+l} \alpha^l \\ & + \sum_{l=1}^{L-1} \omega^l (Z \cdot \gamma^{l+1} + \alpha^{l+1} - Z\gamma^l - \alpha^l) \\ & + \sum_{l=1}^L \lambda^l (Z \cdot \gamma^l - 1 - \beta^l) \end{aligned} \quad (45)$$

For notational convenience, we set  $\alpha^L = 0$  and  $\omega^0 = 0$ . We reorder the terms of the Lagrangian in terms of summations over the primal variable indices.

$$\begin{aligned} \min_{\substack{\gamma \geq 0 \\ \beta \geq 0 \\ \alpha \geq 0}} \max_{\omega \geq 0, \lambda \geq 0} & \sum_{l=1}^L -\lambda^l 1 + \sum_{l=1}^L (-\theta^{-l} - \lambda^l) \beta^l \\ & + \sum_{l=1}^L (\theta^{+l} + \omega^{l-1} - \omega^l) \alpha^l + \sum_{l=1}^L (\theta^l + \lambda^l + \omega^{l-1} - \omega^l) \cdot Z \gamma^l \end{aligned} \quad (46)$$

Each primal variable yields a positivity constraint in the dual.

$$\begin{aligned} \max_{\omega \geq 0, \lambda \geq 0} & \sum_{l=1}^L -\lambda^l 1 \\ \text{s.t. } & (-\theta^{-l} - \lambda^l) \geq 0 \quad \forall l \\ & (\theta^{+l} - \omega^l + \omega^{l-1}) \geq 0 \quad \forall l \\ & (\theta^l + \lambda^l + \omega^{l-1} - \omega^l) \cdot Z \geq 0 \quad \forall l \end{aligned} \quad (47)$$

This dual LP can be interpreted as finding modification of the original edge weights  $\theta^l$  so that every possible cut of each resulting graph has non-negative weight. Observe that the introduction of the two slack terms  $\alpha$  and  $\beta$  in the primal problem (Eq 11) results in bounds on the Lagrange multipliers  $\lambda$  and  $\omega$  in the dual problem in Eq 47. The constraint  $(-\theta^{-l} - \lambda^l) \geq 0$  is a result of the introduction of  $\beta^l$ . The constraint  $\omega^{l-1} - \omega^l \leq \theta^{+l}$  is a result of the introduction of  $\alpha^l$ . In practice these bounds turn out to be essential for efficient optimization and are a key contribution of this paper.

It is also informative to make the substitution  $\mu^l = \omega^l - \omega^{l-1}$  which yields a slightly more symmetric formulation

$$\max \sum_{l=1}^L -\lambda^l 1 \quad (48)$$

$$\begin{aligned} \text{s.t. } & 0 \leq \lambda^l \leq -\theta^{-l} \quad \forall l \\ & 0 \leq \sum_{m=1}^l \mu^m \quad \forall l \\ & \mu^l \leq \theta^{+l} \quad \forall l \\ & (\theta^l + \lambda^l - \mu^l) \cdot Z \geq 0 \quad \forall l \end{aligned} \quad (49)$$

## D Producing a genuine lower bound on the optimal integer solution

Consider optimizing the Lagrangian over the set of integer solutions  $\mathcal{X} \in \bar{\Omega}_L$ . In this case the  $\alpha, \beta$  terms disappear. For a given setting of the remaining multipliers  $\omega, \lambda$  we have a lower bound on the

optimal integer solution given by:

$$\begin{aligned}
L(\omega, \lambda) &= \min_{\mathcal{X} \in \bar{\Omega}_L} \sum_{l=1}^L (\theta^l \bar{X}^l + \omega^l (\bar{X}^{l+1} - \bar{X}^l) + \lambda^l (\bar{X}^l - 1)) \\
&= \min_{\mathcal{X} \in \bar{\Omega}_L} \sum_{l=1}^L (\theta^l \bar{X}^l + \omega^{l-1} \bar{X}^l - \omega^l \bar{X}^l + \lambda^l \bar{X}^l - \lambda^l 1) \\
&= \min_{\mathcal{X} \in \bar{\Omega}_L} \sum_{l=1}^L (\theta^l + \omega^{l-1} - \omega^l + \lambda^l) \bar{X}^l - \lambda^l 1 \\
&= \sum_{l=1}^L -\lambda^l 1 + \min_{\mathcal{X} \in \bar{\Omega}_L} \sum_{l=1}^L (\theta^l + \omega^{l-1} - \omega^l + \lambda^l) \bar{X}^l \\
&\geq \sum_{l=1}^L -\lambda^l 1 + \sum_{l=1}^L \min_{X^l \in \text{MCUT}} (\theta^l + \omega^{l-1} - \omega^l + \lambda^l) \bar{X}^l \\
&\geq \sum_{l=1}^L -\lambda^l 1 + \sum_{l=1}^L \frac{3}{2} \min_{\bar{X}^l \in \text{CUT}} (\theta^l + \omega^{l-1} - \omega^l + \lambda^l) \bar{X}^l
\end{aligned} \tag{50}$$

where the first inequality arises from dropping the constraints between layers of the hierarchy and the second inequality holds for planar graphs where the the optimal multi-cut is bounded below by  $\frac{3}{2}$  the value of the optimal two-way cut (see [20]).